THE JOURNAL OF PHYSICAL CHEMISTRY B

 VOLUME 107, NUMBER 46, NOVEMBER 20, 2003

LETTERS

In Situ Raman Spectroscopy of Single Microparticle Li^+−Intercalation Electrodes

Kaoru Dokko, Qingfang Shi, Ionel C. Stefan, and Daniel A. Scherson*

Department of Chemistry, Case Western Reserve University, Cleveland, Ohio 44106-7078

Received: April 11, 2003; In Final Form: July 30, 2003

Modifications in the vibrational properties of a single microparticle of $LiMn_2O_4$ induced by extraction and subsequent injection of Li^+ into the lattice have been monitored in situ via *simultaneous* acquisition of Raman scattering spectra and cyclic voltammetry data in 1 M $LiClO_4$ solutions in ethylene carbonate (EC):diethyl carbonate (DEC) mixtures (1:1 by volume). Statistical analyses of the spectra in the range 15 < SOD < 45%, where SOD represents the state of discharge (in percent) of the nominally fully charged material, i.e., λ-MnO_2, were found to be consistent with the coexistence of two distinct phases of lithiated metal oxide in agreement with information derived from in situ X-ray diffraction (XRD) measurements involving more conventional battery-type electrodes (*J. Electrochem. Soc.* **2002**, *149*, A1164).

Introduction

The development of in situ techniques for the characterization of the intrinsic properties of charge storage materials is expected to play a key role toward elucidating the factors that control important aspects of battery electrodes, including structural changes induced by charge and discharge, as well as capacity fade effects upon repeated cycling. Efforts are being made in several laboratories to eliminate possible interferences derived from the presence of additives, such as conductivity enhancers and binders, which may compromise reliable quantitative data analyses. Indeed, several schemes have been described in the literature for performing measurements on pure charge storage materials supported on inert conducting substrates, either as films[1−7] or as single[8−10,11] or ensembles of particles,[12−16] of the same type as those used in commercial devices. Particularly noteworthy is the work of Uchida and co-workers involving electrochemical measurements on single particle electrodes,[8−11] as well as that of our group at CWRU, which relies on the mechanical embedding of technical microparticles on either gold or nickel supports to examine in situ vibrational[13,12,16] and electronic and structural properties[17,14] of Li^+-insertion electrodes as a function of their states of charge. Although important information has been derived from the analysis of results obtained from such experiments, it has not been possible so far to perform *simultaneously* spectroscopic and electrochemical measurements on single particle electrodes. This paper describes a novel experimental strategy that enables in situ Raman spectra of a single microparticle to be acquired while recording cyclic voltammograms at low scan rates, using $LiMn_2O_4$ in a Li^+-containing organic electrolyte as a model system. Key to the success of these experiments was the combined use of a microelectrode to both contact electrically and press mechanically the microparticle against an optical window, an airtight spectroelectrochemical cell, and a Raman microscope to focus the exciting laser radiation directly on the surface of the microparticle, while collecting the scattered light by the same objective lens.

Experimental Section

A schematic diagram of the all-glass, airtight, spectroelectrochemical cell, as well as of the overall experimental arrangement for in situ Raman spectroscopy of single particle microelectrodes is depicted in panel A, Figure 1. As indicated therein, the cell is equipped with a sapphire window (Escoproducts Inc., 0.5 mm thick) sealed against the cell body with an O-ring (KALREZ) using a metal clamp, and with a Li metal foil (2

* Corresponding author.

10.1021/jp034977c CCC: $25.00
Published on Web 10/23/2003

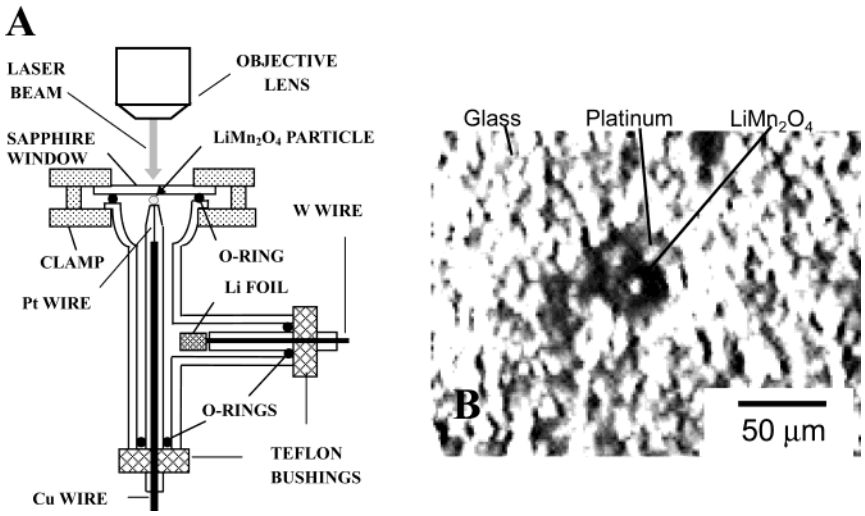

Figure 1. Schematic diagram of the spectroelectrochemical cell employed in these studies for the acquisition of simultaneous in situ Raman and cyclic voltammetric measurements of a single particle microelectrode (panel A). Shown in panel B in this figure is a photograph acquired with the microscope attachment of the small area of the microelectrode including the Pt electrode the $LiMn_2O_4$ microparticle and the surrounding glass casing.

cm^2) pressed against a tungsten wire as a counter/reference electrode. Electrical contact to the microparticle was achieved with a Pt microelectrode prepared by sealing the tip of a Pt wire (50 μm in diameter) into a Pyrex glass tube using a hydrogen flame, which was later polished with sandpaper (CARBIMET, GRIT 600) to expose a circularly shaped electrode. The other end of the Pt wire was attached to a much thicker Cu wire, which was used in turn as an external electrical contact. Prior to cell assembly, the microelectrode was pushed against the sapphire window and fixed firmly in that position using a Teflon bushing. The window was then detached from the cell, and a single $LiMn_2O_4$ particle (ca. 25 μm in diameter, Rayovac Corp.) placed in the center of the microelectrode (see panel B, Figure 1) utilizing the tip of a sharp needle as a manipulator under a conventional optical microscope. The window was once again mounted onto the cell body pressing the particle against the surface of the Pt disk with high enough force to keep it rigidly in position without compromising its integrity. At this stage, the cell was transferred to a glovebox (Vacuum Atmospheres) equipped with water and oxygen sensors, where it was later filled with a 1 M $LiClO_4$ solution in a mixture of ethylene carbonate (EC) and diethyl carbonate (DEC) (1:1 by volume). Once carefully sealed, the cell was removed from the glovebox and placed directly beneath the microscope objective of the Raman microscope (see below).

Raman spectra were acquired using a Raman 2000 system (Chromex Inc., Albuquerque, NM) equipped with a microscope attachment, using the same optical setup described elsewhere.[12] A focused (20X Olympus microscope) 532 nm laser beam (Verdi, Coherent) impinging onto the $LiMn_2O_4$ particle at near normal incidence (beam spot size on the particle ca. 5 μm diameter, see panel B, Figure 1), was used as the excitation source at powers low enough to avoid photothermal damage, and the scattered light was collected by the microscope objective. A Super-Notch-Plus filter (Kaiser Optical Systems, Inc., Ann Arbor, MI) placed just before the spectrograph stage was used to remove the primary beam. All data were obtained with the slit width set at 50 μm, with a spectral resolution of 2 cm^{-1}. A forced air-cooled charge coupled device (CCD) camera with 1024 $\times$ 256 pixels (Photometrics, Roper Scientific, Tucson, AZ) was employed as a detector. The integration time for each frame was 15 s with four frames co-added to improve the signal-to-noise ratio. Spectral contributions due to the sapphire window and the electrolyte were subtracted using commercial software (Origin). The electrode potential was controlled with a conventional potentiostat (AFRDE5, Pine Instruments), and all measurements were carried out at room temperature. Two complete cyclic voltammograms (not shown here) in the potential range $3.60 < E < 4.40$ V vs Li/Li^+ starting at the negative limit, followed by a single linear scan ending at the positive limit were recorded at a scan rate $\nu = 0.5$ mV/s for each particle with the cell placed under the Raman microscope prior to the spectroelectrochemical experiments. Immediately thereafter, the scan rate was reduced to ca. $\nu = 0.11$ mV/s and a complete cyclic voltammogram collected in the range 4.40−3.60 V while acquiring continuously in situ Raman spectra. Careful monitoring of the potential as a function of time during the voltammetric cycle (by recording real times during voltage data collection) revealed slight differences between the scan rates in the positive and negative directions (although the scans in each direction were indeed highly linear). For this reason, the current/potential data collected in this work were normalized by dividing the current corresponding to each individual linear scan by the appropriate scan rate and are thus displayed as capacitance vs potential plots (see below). Spectra were collected and coadded over a 60 s interval to yield signals averaged over a potential range of ca. 7 mV and then stored for further processing. The composition of the lithiated manganese oxide material within the phase 1 and phase 2 transition region was determined from the spectroscopic data using the LC XANES routine of WinXAS, an extended X-ray absorption fine structure analysis package. This program relies on statistical fitting methods and spectral additivity to determine the composition of a mixture, e.g. A + B, using as input the experimentally recorded spectra of the pure constituent phases A and B, allowing direct comparison with data derived from coulometric analyses.

Results and Discussion

Capacitance vs potential data for the single $LiMn_2O_4$ particle collected in the spectroelectrochemical cell in the range 4.40−3.60 V at ca. $\nu = 0.11$ mV/s (see above), *while* acquiring continuously Raman spectra, are shown in Figure 2. As indicated therein, the curve displayed two clearly defined sets of complementary peaks centered at around 4.0 (A/A′) and 4.1 V

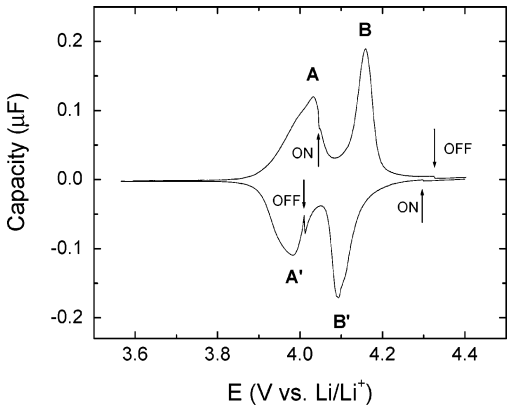

Figure 2. Capacity vs *E* data extracted from the cyclic voltammogram (CV) of a single $LiMn_2O_4$ microparticle recorded at a scan rate of ca. 0.11 mV/s (see text for details) in a 1 M $LiClO_4$ solution in a mixture of ethylene carbonate (EC) and diethyl carbonate (DEC) (1:1 by volume) in the spectroelectrochemical cell *during* acquisition of Raman spectra. The exciting focused laser beam was turn ON and OFF at the potentials specified by the arrows in the curve.

(B/B′) vs Li/Li^+ in excellent agreement with data published elsewhere.[9] As has also been discussed thoroughly in the literature,[18] the charge under each of these peaks corresponds to about half the total amount of Li^+ in $LiMn_2O_4$ to yield, in sequence, $Li_{0.5}Mn_2O_4$ and λ-MnO_2. The differences in the values of the peak potentials between complementary features observed in the scan in the positive and negative directions (Figure 2) are somewhat smaller than those reported earlier by Luo et al. in our laboratory,[13] indicating that the *iR* drop in the present configuration is far reduced despite the fact that the single particle electrode is actually touching the window. Also responsible for at least part of the hysteresis is the very small diffusion coefficient of Li^+ within the metal oxide lattice, which renders the system under partial (solid state) mass transport control even at the slow scan rate employed for these experiments. In view of the rather weak Raman signals observed between 3.6 and 4.0 V (not shown here), the laser was turned off while scanning within this range to avoid unnecessary heating of the particle. The slight changes in the current observed upon turning the laser on and off (see Figure 2) are due to

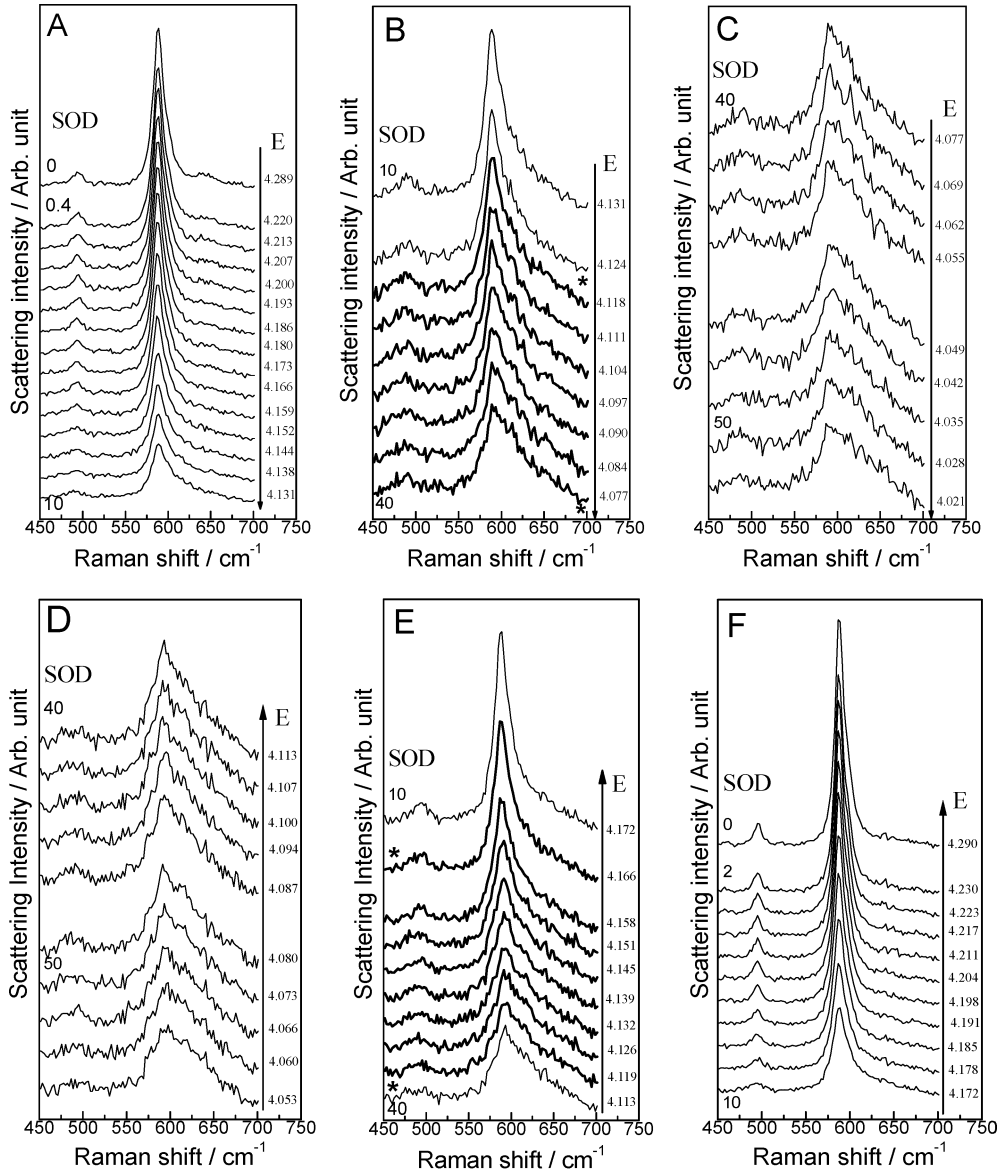

Figure 3. Series of Raman spectra recorded while acquiring the cyclic voltammetry data for the single $LiMn_2O_4$ microparticle shown as capacity vs *E* in Figure 2 for the scan in the negative (panels A−C) and positive (panels D−F) directions. The average potential, *E*, during each spectral collection is indicated on the right, whereas selected values of the state of discharge (SOD, %) are shown on the left side of the curves. The spectra in thicker lines were used for quantitative analyses of phase composition (see Figure 5).

photoexcitation processes, which are at least in part responsible for the slight imbalance in the charge observed between the scans in the positive and negative directions (see below).

In situ potential-averaged Raman spectra acquired *continuously* during that third linear scan in the negative, and subsequent positive directions are shown in the upper (A−C) and lower panels (D−F) in Figure 3, respectively, where the numbers on the right of each of the traces represent the average potential during spectral collection. As has been noted by other workers, the Raman features of $LiMn_2O_4$ are of much weaker intensities than those of $Li_{0.5}Mn_2O_4$ or the nominally fully delithiated material, λ-MnO_2; hence, no attempt was made to analyze data in the potential range $E < 4.021$ V vs Li/Li^+. Although lacking much resolution, the broad, and markedly asymmetric feature centered at ca. 600 cm^{-1} found for $4.021 < E < 4.118$ V can be ascribed to two T_2 and two A_1 modes of $Li_{0.5}Mn_2O_4$. Two prominent peaks centered at 495, and particularly at 588 cm^{-1}, attributed to the $T_{2g}(2)$ and A_{1g} modes of λ-MnO_2, respectively, could be discerned in the spectra collected for $E > 4.131$ V (see panels A and B, Figure 3). Quantum mechanical calculations[19] predict additional Raman active bands for this specific material at 479 cm^{-1}, E_g, and 630 cm^{-1}, $T_{2g}(3)$. Although both of these modes have been observed by other workers[19,20] (at i.e., 463 and 647 cm^{-1}, respectively), their presence could not be clearly identified in our in situ spectra owing probably to their lower Raman scattering cross sections. The increase in scattering intensity in the region of 450−700 cm^{-1} for $E > 4.172$ V (up to 4.29 V;see panel C) is due to resonance enhancement effects associated with λ-MnO_2 at the excitation wavelength employed in these experiments.[19] A similar overall trend was found for spectra recorded during charging, as shown in panels D−F in Figure 3.

At least three factors must be considered before a quantitative analysis of the data collected can be pursued:

i. According to reports published in the literature,[21] the theoretical capacity of $LiMn_2O_4$ exceeds by about 20% the values found experimentally implying that a rather significant fraction of Li^+ is retained by the lattice even when the material is nominally fully charged.

ii. The total charge storage capacity of the microparticle examined, as measured via integration of the current in the scan in the negative direction, yielded a value of ca. 23.18 μC (see panel A, Figure 4) and thus less than ca. 3% larger than the total charge released determined by a similar coulometric analysis of the subsequent scan in the positive direction, i.e., 22.54 μC. Such a small imbalance is most likely derived from photocurrents induced by laser irradiation, which were negative in most of the potential range in which the redox transitions were found to occur and will not be considered in the analysis to follow.

iii. The scan rate employed in these specific measurements (ca. $\nu = 0.11$ mV/s) was higher than that required for the microparticle to achieve full equilibration at any given potential, leading to slight distortions in the charge vs potential curves. In fact, even under these less than optimum conditions, a complete set of spectroelectrochemical measurements, (i.e., spectral acquisition during a full voltammetric cycle) took in excess of 4 h. It must be stressed, however, that in view of the small diffusion coefficient of Li^+ within the metal oxide lattice, and the rather small penetration depth of the beam, the spectral measurements are expected to represent rather accurately those of a particle in equilibrium with the applied potential.

It will be assumed in what follows, that the state of discharge (SOD in %) of the $LiMn_2O_4$ electrode is defined as zero when

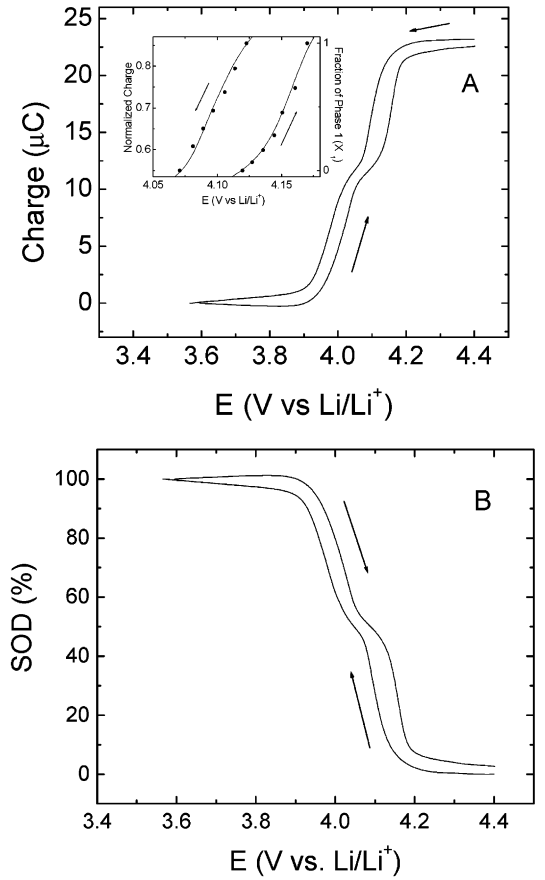

Figure 4. Plots of charge vs potential (E) (panel A) and state of discharge (SOD) vs E (panel B) based on coulometric analyses of the capacity vs E data in Figure 2. The insert panel A displays the same data in the form of normalized change, Q/Q_{total}, where Q_{total} is the charge measured during complete discharge, ca. 23 μC as a function of potential. The right axis in this plot represents the fraction of phase 1 present in the material, X_1, and the solid circles the magnitudes of X_1 at the specified potentials, as calculated from the component analysis of the spectroscopic data in Figure 6 (see text for details).

the microparticle is polarized at the most positive potential, i.e., $E = 4.30$ V, and that its full capacity (one Li^+ per electron) corresponds to the charge released upon full nominal discharge (integration of the voltammetric curve down to $E = 3.60$ V). On this basis, it becomes possible to construct plots of SOD as a function of E, as shown in panel B, Figure 4, and to correlate these data (uncorrected for photoinduced effects) with information derived from the spectroscopic measurements recorded *simultaneously*.

Of particular relevance to this study are the in situ X-ray diffraction (XRD) measurements reported by Eriksson et al.[22] for $Li_xMn_2O_4$, which are consistent with the presence of one single phase, denoted as 1, over the range $0 < SOD < 11\%$ (phase 1) and a different single phase (phase 2) over $35 < SOD < 100\%$. Evidence was also obtained by these workers for the coexistence these two phases in the intermediate range $11 < SOD < 35\%$, for which their respective lattice parameters remained fixed at 8.805 Å (phase 1) and 8.145 Å (phase 2). As shown in panel A, Figure 3, large drops in intensity were found in the Raman spectra recorded during the initial stages of discharge of the fully charged microparticle in which the only phase present (phase 1) undergoes a linear lattice expansion as a function of the SOD. This behavior is in all likelihood related to changes in the electronic properties of the material as Li^+ is injected into the lattice, leading to a rapid loss of resonantly

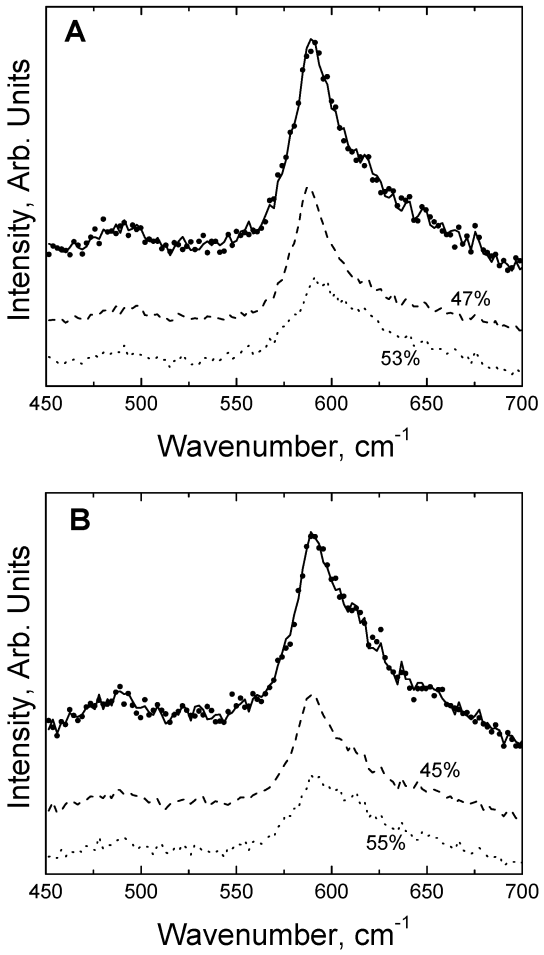

Figure 5. Detailed statistical fits (see solid line through to the actual experimental Raman spectra in scattered points in the upper curves in each panel) to the Raman data collected at 4.151 V during the positive scan (panel A) and 4.097 V during the negative scan (panel B). The bottom curves in each of the panels represent *to scale* the individual contributions from the two pure phases, i.e., SOD = 16% (E = 4.166 V) for phase 1, and SOD = 45% (E = 4.126 V) for phase 2 in panel A, and SOD = 16% (E = 4.118) V for phase 1, and SOD = 43% (E = 4.077 V) for phase 2 in panel B. The values adjacent to each of the lower curves in panels A and B correspond to the best-fit percents of each of the phases at the specified potential.

enhanced intensity associated with λ-MnO_2, a phenomenon that complicates a more quantitative interpretation of spectra recorded in this SOD region.

More amenable to a rigorous analysis, however, are spectral data acquired in the intermediate SOD range, where as stated above, the lattice parameters of the two phases are independent of the SOD. To this end, the Raman spectra collected at SOD = ca. 16% and ca. 43% were assumed to represent the pure phases 1 and 2, respectively, and *no restrictions were imposed while fitting the data on the sum of the constituent phases for each SOD*. Spectra used for analysis are indicated by thicker lines and pure phases by a star in panels B and E, Figure 3. Two typical examples of fits to the spectra are shown in panels A and B, Figure 5, which display both the contributions made by each of the two pure phases (phase 1 as dashed line and phase 2 as dotted line), as well as their sum (see continuous line superimposed on the scattered experimental points), for spectra recorded during the positive scan at 4.151 V (panel A) and the negative scan at 4.097 V (panel B). The values indicated in each of the curves represent the percent of each of the phases in the specimen as determined from the mathematical analysis.

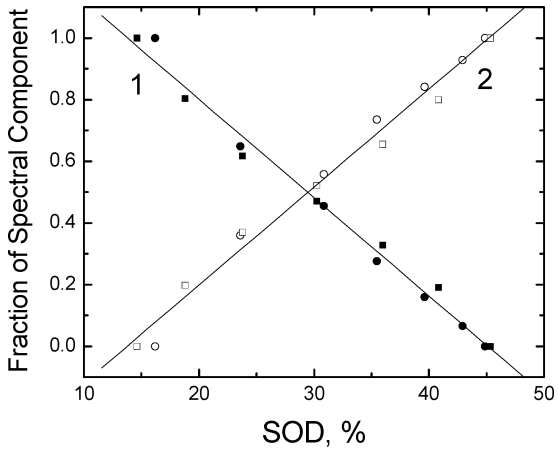

Figure 6. Plots of the fraction of the spectral component for phase 1 (solid symbols) and phase 2 (open symbols) for data collected during the scan in the negative (circles) and positive (squares) directions based on a statistical analysis of the spectra shown in thick lines in Figure 3. The sum of the contributions of each of the two spectrally determined phases to the total Raman spectra was 1 ± 0.02, whereas the linear fits to the data yielded R values larger than 99%.

In analogy with the conclusions made by Eriksson et al.[22] based on their in situ XRD studies, the results derived from the statistical treatment of the Raman data for the microparticle yielded good linear correlations (R > 0.99) between the fraction of each constituent phase and the SOD (see Figure 6). Furthermore, the *unrestricted* sum of the components correctly predicts (within 2%) values very close to 1, lending strong support to the validity of the method implemented. A very clear illustration of the direct correlation that can be drawn between purely electrochemical and in situ spectroscopic data is given in the insert Figure 4, where the left axis is the normalized charge, i.e., Q/Q_{total}, where Q_{total} is the charge measured during complete discharge, ca. 23 μC, as a function of potential, the right axis represents the fraction of phase 1 present in the material, X_1, and the solid circles are the magnitudes of X_1 at the specified potentials, as calculated from the component analysis of the spectroscopic data in Figure 6 (text for details). As indicated, the two sets of data are indeed in excellent agreement.

Conclusions

Simultaneous in situ Raman spectroscopic and electrochemical measurements of a single particle of $LiMn_2O_4$ (25 μm diameter) attached to a Pt microdisk were successfully performed using a Raman microscope and a specially designed spectroelectrochemical cell. Statistical analysis of the data obtained yielded results consistent with information derived from XRD making it possible to correlate optical data with phase composition for SOD values in the range 11 and 35%. Slight modifications to the methods described will make it possible to extend measurements of the type herein presented to a wide variety of energy storage materials, including graphite. The results emerging from such measurements will allow direct correlations to be made between the state of charge of single particle electrodes and their Raman spectroscopic properties, thereby providing means of monitoring spatiotemporal effects induced by intercalation electrodes of interest to the operation and performance of energy storage devices.

Acknowledgment. This work was supported in part by NASA-Glenn and the US Department of Energy, Office of Basic Energy Sciences. Additional funding was provided by Eveready

Battery Co., Westlake, OH. K.D wishes to express his deep appreciation to Prof. Isamu Uchida (Tohoku University) for his helpful comments. K.D. acknowledges a research fellowship from the Japan Society for the Promotion of Science. The authors wish to also acknowledge one of the reviewers who suggested the display of the spectroscopic derived data directly onto the coulometric curves.

References and Notes

(1) Anzue, N.; Itoh, T.; Mohamedi, M.; Umeda, M.; Uchida, I. *Solid State Ionics* **2003**, *156*, 301−307.

(2) Desilvestro, J.; Corrigan, D. A.; Weaver, M. J. *J. Phys. Chem.* **1986**, *90*, 6408−6411.

(3) Desilvestro, J.; Corrigan, D. A.; Weaver, M. J. *J. Electrochem. Soc.* **1988**, *135*, 885−892.

(4) Dokko, K.; Mohamedi, M.; Anzue, N.; Itoh, T.; Uchida, I. *J. Mater. Chem.* **2002**, *12*, 3688−3693.

(5) Yamamura, S.; Koshika, H.; Nishizawa, M.; Matsue, T.; Uchida, I. *J. Solid-State Electrochem.* **1998**, *2*, 211−215.

(6) Nishizawa, M.; Ise, T.; Koshika, H.; Itoh, T.; Uchida, I. *Chem. Mater.* **2000**, *12*, 1367−1371.

(7) Mohamedi, M.; Takahashi, D.; Uchiyama, T.; Itoh, T.; Nishizawa, M.; Uchida, I. *J. Power Sources* **2001**, *93*, 93−103.

(8) Dokko, K.; Horikoshi, S.; Itoh, T.; Nishizawa, M.; Mohamedi, M.; Uchida, I. *J. Power Sources* **2000**, *90*, 109−115.

(9) Dokko, K.; Nishizawa, M.; Mohamedi, M.; Umeda, M.; Uchida, I.; Akimoto, J.; Takahashi, Y.; Gotoh, Y.; Mizuta, S. *Electrochem. Solid State Lett.* **2001**, *4*, A151-A153.

(10) Dokko, K.; Mohamedi, M.; Umeda, M.; Uchida, I. *J. Electrochem. Soc.* **2003**, *150*, A425-A429.

(11) Uchida, I.; Mohamedi, M.; Dokko, K.; Nishizawa, M.; Itoh, T.; Umeda, M. *J. Power Sources* **2001**, *97*−*8*, 518−524.

(12) Luo, Y.; Cai, W. B.; Scherson, D. A. *J. Electrochem. Soc.* **2002**, *149*, A1100-A1105.

(13) Luo, Y.; Cai, W.-B.; Scherson, D. A. *Electrochem. Solid State Lett.* **2001**, *4*, A101-A104.

(14) Totir, D. A.; Bae, I. T.; Hu, Y. N.; Antonio, M. R.; Stan, M. A.; Scherson, D. A. *J. Phys. Chem. B* **1997**, *101*, 9751−9756.

(15) Totir, D. A.; Cahan, B. D.; Scherson, D. A. *Electrochim. Acta* **1999**, *45*, 161−166.

(16) Totir, D. A.; Scherson, D. A. *Electrochem. Solid State Lett.* **2000**, *3*, 263−265.

(17) Totir, D. A.; Antonio, M. R.; Schilling, P.; Tittsworth, R.; Scherson, D. A. *Electrochim. Acta* **2002**, *47*, 3195−3200.

(18) Gao, Y.; Reimers, J. N.; Dahn, J. R. *Phys. Rev. B* **1996**, *54*, 3878−3883.

(19) Ammundsen, B.; Burns, G. R.; Islam, M. S.; Kanoh, H.; Roziere, J. *J. Phys. Chem. B* **1999**, *103*, 5175−5180.

(20) Kanoh, H.; Tang, W. P.; Ooi, K. *Electrochem. Solid State Lett.* **1998**, *1*, 17−19.

(21) Thackeray, M. M. *Prog. Solid State Chem.* **1997**, *25*, 1−71.

(22) Eriksson, T.; Hjelm, A. K.; Lindbergh, G.; Gustafsson, T. *J. Electrochem. Soc.* **2002**, *149*, A1164.